

Polyelectrolyte Electrophoresis in Nanochannels: A Dissipative Particle Dynamics Simulation

Jens Smiatek^{1,*} and Friederike Schmid^{2,†}

¹*Institut für Physikalische Chemie, Universität Münster, D-48149 Münster, Germany*

²*Institut für Physik, Johannes Gutenberg-Universität, Staudinger Weg 7, D-55099 Mainz, Germany*

(Dated: January 6, 2010)

We present mesoscopic DPD-simulations of polyelectrolyte electrophoresis in confined nanogeometries, for varying salt concentration and surface slip conditions. Special attention is given to the influence of electroosmotic flow (EOF) on the migration of the polyelectrolyte. The effective polyelectrolyte mobility is found to depend strongly on the boundary properties, *i.e.*, the slip length and the width of the electric double layer. Analytic expressions for the electroosmotic mobility and the total mobility are derived which are in good agreement with the numerical results. The relevant quantity characterizing the effect of slippage is found to be the dimensionless quantity $\kappa \delta_B$, where δ_B is the slip length, and κ^{-1} an effective electrostatic screening length at the channel boundaries.

PACS numbers: 82.35.Rs 47.57.jd 47.61.-k 82.45.+z 83.50.Lh

I. INTRODUCTION

In recent years there is growing interest in techniques for manipulating single nanoparticles or macromolecules in micro- and nanochannel systems. The flow profiles in these channels and the motion of the macromolecules can be controlled on the nanoscale by pressure gradients and electric fields, and by exploiting smart channel geometries. This explains the great potential and the broad applicability of nanochannel devices, *e.g.*, for analyzing tiny DNA or protein samples by electrophoresis^{1–11}.

Such systems represent a challenge for theory and computer simulation due to their high complexity. In biotechnological applications, the molecules of interest are often charged and dissolved in buffer solutions with high salt concentrations. Thus electrostatic and hydrodynamic effects compete with each other, resulting, among other, in a remarkable ‘electrohydrodynamic screening’ effect: In free solution electrophoresis (*i.e.*, in a constant electric field), the counterion layer surrounding a charged particle not only screens the electrostatic interactions, but also the dominant contribution to the hydrodynamic interactions, *i.e.*, those that are generated by the applied field^{12,13}. Therefore, simulations of electrophoresis that neglect the electrostatic and hydrodynamic interactions altogether often give results that are in good semiquantitative agreement with experiments^{1,14,15}. More sophisticated approaches that still allow to avoid the explicit representation of charges have been devised as well^{16,17}. Nevertheless, it is clear that such simplified treatments disregard important physics, especially in confined geometries where electrostatic interactions compete with the regular steric interactions with the confining walls¹⁸. Simulations that take full account of electrostatic and hydrodynamic interactions are clearly desirable. Such simulations have recently been carried out for polyelectrolyte electrophoresis in free solutions^{19,20}, but, to the best knowledge of the present authors, not yet for microchannels.

In many microchannels, an additional effect comes into play, which significantly modifies the effective electrophoretic response of particles to electric fields: The same electric field that drives the polyelectrolyte may also induce a total net fluid flow in the microchannel, the ‘electroosmotic flow’ (EOF). Many materials commonly used in microtechnology like PDMS (Polydimethylsiloxane) acquire charges if brought in contact with water, either by the ionization or dissociation of surface groups or the adsorption of ions from solution. To screen the charges on the channel walls, a diffuse layer of oppositely charged ions forms in front of the walls. In the presence of an external electric field $\mathbf{E}^{(ext)}$, these ions are pulled along, dragging the surrounding fluid with them. One gets a characteristic ‘plug’ flow profile which saturates at a fluid velocity

$$\mathbf{v}_{\text{EOF}} = \mu_{\text{EOF}} \mathbf{E}^{(ext)} \quad (1)$$

outside of the diffuse layer, with the so-called electroosmotic mobility μ_{EOF} . The effective migration speed \mathbf{v}_P of particles in microchannels in response to the external fields then results from two contributions¹⁵: The bare electrophoretic mobility μ_e of the polyelectrolyte in a fluid at rest, and the background EOF velocity, $\mathbf{v}_P = \mathbf{v}_{\text{EOF}} + \mu_e \mathbf{E}^{(ext)}$. Experimentally, it has been found that the former may even dominate over the latter, such that the polyelectrolyte effectively migrates in the direction *opposite* to the applied field⁴.

Now if the diffuse layer is thin compared to the channel dimensions, Eq. (1) can be regarded as an effective boundary condition for a steady-state EOF velocity field $\mathbf{v}_{\text{EOF}}(\mathbf{r})$ inside the channel. (We note that in a steady-state situation, the external field in the vicinity to a wall is necessary parallel to the wall.) Cummings et al.²¹ have shown that for laminar incompressible flow, this boundary condition effectively defines the flow inside the channel. Provided Eq. (1) also holds at the inlet and outlet boundaries of the channel, it becomes valid everywhere in the channel²². Due to this remarkable similitude between the steady-state velocity field of an EOF and the

externally applied electric field, the net electrophoretic velocity of nanoparticles or polyelectrolytes can be written approximately as

$$\mathbf{v}_P = (\mu_{\text{EOF}} + \mu_e) \mathbf{E}^{(ext)} =: \mu_t \mathbf{E}^{(ext)} \quad (2)$$

with the effective total mobility $\mu_t = \mu_{\text{EOF}} + \mu_e$. We note that this expression relies on two assumptions which are both not obvious: The nanoparticles or polyelectrolytes stay well outside the diffuse layer covering the wall, and they themselves do not influence the EOF.

The EOF amplitude at planar walls with no-slip boundary conditions has been calculated a long time ago by Smoluchowski²³. On the nanoscale, however, the no-slip boundary condition does not necessarily apply. Experiments have indicated^{24–26}, that the velocity profile is not strictly continuous at walls, *i.e.*, fluids exhibit a certain amount of slippage. This effect can be enhanced significantly by using superhydrophobic walls which are covered by a thin gas layer. It can also be tuned to some extent by designing nanopatterned surfaces with alternating hydrophobic and hydrophilic sections²⁷. In all of these cases, the appropriate mesoscopic boundary condition is the ‘partial slip’ boundary condition,

$$v_x(\pm z_B) = \mp \delta_B \frac{\partial}{\partial z} v_x(z)|_{z=\pm z_B}, \quad (3)$$

where z_B is the position of the hydrodynamic boundary (which is usually close to the physical boundary, but not necessarily identical), and the ‘slip length’ δ_B characterizes the amount of slippage. No-slip boundaries correspond to $\delta_B = 0$, full-slip to $\delta_B \rightarrow \infty$. From Eq. (3), one would expect that the EOF amplitude is enhanced in the presence of slippage²⁷, and this is indeed found in simulations^{28,29}. The effect of slippage on EOF has been calculated within the linearized Poisson-Boltzmann theory, the Debye-Hückel approximation, by Joly et al.²⁸. Below, we will derive a general expression which is also valid beyond the Poisson-Boltzmann theory.

In this paper we present Dissipative Particle Dynamics (DPD)-simulations of polyelectrolyte electrophoresis in microchannels with varying slip lengths, at varying salt concentrations. We treat the solvent and all ions explicitly, and all charges interact *via* unscreened Coulomb interactions. This allows to investigate the interplay of solvent and polyelectrolyte, of electrostatic and hydrodynamic interactions, of electrophoresis and EOF in full detail, with almost no approximation. (Our only approximation is to neglect image charge effects, *i.e.*, the dielectric constant is taken to constant everywhere.) Our results indicate that the hydrodynamic boundary conditions strongly influence the total mobility of the polyelectrolyte, and the total mobility can be tuned from positive to negative by varying the slip length. The simulation data are compared with a simple analytical expression, which is derived based on the assumption that the flow profile in the channel follows the Stokes equation. The numerical results are in very good agreement with the theory.

The paper is organized as follows. The theory is presented in section 2. Section 3 focuses on the simulation method and the parameters used in our simulations. The numerical results will be shown in section 4. We conclude with a brief summary in section 5.

II. THEORETICAL CONSIDERATIONS: EOF IN THE PRESENCE OF SLIPPAGE

We consider for simplicity a planar slit channel with identical walls at $z = \pm L/2$, exposed to an external electric field E_x in the x direction. The electrostatic potential $\Phi(x, y, z)$ then takes the general form $\Phi(x, y, z) = \psi(z) + E_x x + \text{const.}$ where we can set $\psi(0) = 0$ for simplicity. The electrolyte in the channel is taken to contain n different ion species i with local number density $\rho_i(z)$ and valency Z_i , which results in a net charge density $\rho(z) = \sum_{i=1}^n (Z_i e) \rho_i(z)$. The electric field then generates a force density $f_x(z) = \rho(z) E_x$ in the fluid. Comparing the Poisson equation for the electrostatic potential ψ ,

$$\frac{\partial^2 \psi(z)}{\partial z^2} = -\frac{\rho(z)}{\epsilon_r} \quad (4)$$

(where ϵ_r is the dielectric constant), with the Stokes equation³⁰

$$\eta_s \frac{\partial^2 v_x(z)}{\partial z^2} = -f_x(z) = -\rho(z) E_x \quad (5)$$

(with the shear viscosity η_s), one finds immediately $\partial_{zz} v_x(z) = \partial_{zz} \psi(z) (\epsilon_r E_x / \eta_s)$. For symmetry reasons, the profiles v_x and ψ must satisfy the boundary condition $\partial_z v_x|_{z=0} = \partial_z \psi|_{z=0} = 0$ at the center of the channel. This gives the relation

$$v_x(z) = \frac{\epsilon_r E_x}{\eta_s} \psi(z) + v_{\text{EOF}}, \quad (6)$$

where we have used $\psi(0) = 0$ and identified the fluid velocity at the center of the channel with the EOF velocity, $v_x(0) = v_{\text{EOF}}$. We further define $\psi_B := \psi(\pm z_B)$ (for no-slip boundaries, ψ_B is the so-called Zeta-Potential²³). Inserting the partial-slip boundary condition for the flow, Eq. (3), we finally obtain the following simple expression for the electroosmotic mobility,

$$\mu_{\text{EOF}} = v_{\text{EOF}} / E_x = \mu_{\text{EOF}}^0 (1 + \kappa \delta_B), \quad (7)$$

where we have defined the inverse ‘surface screening length’

$$\kappa := \mp \frac{\partial_z \psi}{\psi} \Big|_{z=\pm z_B}, \quad (8)$$

and μ_{EOF}^0 is the well-known Smoluchowski result²³ for the electroosmotic mobility at sticky walls,

$$\mu_{\text{EOF}}^0 = -\epsilon_r \psi_B / \eta_s. \quad (9)$$

The remaining task is to determine the screening parameter κ . If the surface charges are very small and the ions in the liquid are uncorrelated, it can be calculated analytically within the linearized Debye-Hückel theory³¹. The Debye-Hückel equation for the evolution of the potential ψ in an electrolyte solution reads $\partial_{zz}\psi = \kappa_D^2\psi$ with the inverse Debye-Hückel screening length

$$\kappa_D = \sqrt{\frac{\sum_{i=1}^n (Z_i e)^2 \rho_{i,0}}{\epsilon_r k_B T}}, \quad (10)$$

where $\rho_{i,0}$ is the density of ions i far from the surface. It is solved by an exponentially decaying function,

$$\psi(z) \propto (e^{\kappa_D z} + e^{-\kappa_D z} - 2). \quad (11)$$

Inserting that in Eq. (8), one finds $\kappa = \kappa_D$, *i.e.*, the surface screening length is identical with the Debye screening length. Eq. (9) with $\kappa = \kappa_D$ basically corresponds to the result of Joly et al.²⁸.

Unfortunately, the range of validity of the Debye-Hückel theory is limited, it breaks down already for moderate surface potentials ψ_B and/or for highly concentrated ion solutions. Nevertheless, the exponential behavior often persists even in systems where the Debye-Hückel approximation is not valid. For high ion concentrations, detailed studies based on integral equations have lead to the conclusion that the Debye-Hückel approximation can still be used in a wide parameter range, if κ_D is replaced by a modified effective screening length^{32–34}. For high surface charges, analytical solutions are again available in the so-called ‘strong coupling limit’, where the profiles are predicted to decay exponentially with the Guy-Chapman length³⁵. This limit is very special and rarely encountered. At intermediate coupling regimes, the decay length must be obtained empirically, *e.g.*, by fitting the charge distribution $\rho(z)$ to an exponential behavior, which is characterized by the same exponential behavior than $\psi(z)$ by virtue of the Poisson equation,

$$\sum_{i=q}^n (Z_i e) \rho_i(z) \propto \frac{\partial^2 \psi(z)}{\partial z^2} \propto (e^{\kappa z} + e^{-\kappa z}). \quad (12)$$

Putting everything together, the total net electrophoretic mobility μ_t (Eq. 2) of a polyelectrolyte in the channel can be expressed in terms of the electroosmotic mobility μ_{EOF} as

$$\frac{\mu_t}{\mu_{\text{EOF}}} = 1 + \frac{\mu_e}{\mu_{\text{EOF}}^0 (1 + \kappa \delta_B)}, \quad (13)$$

where the ratio μ_e/μ_{EOF}^0 depends only weakly on the ionic strength of the electrolyte and the slip length of the surface. The main effect of slippage is incorporated in the factor $(1 + \kappa \delta_B)^{-1}$.

III. SIMULATION METHOD

A. Dissipative Particle Dynamics

Newtonian fluids are effectively modeled by the Dissipative Particle Dynamics (DPD) method^{36,37}. DPD is a coarse-grained, momentum-conserving simulation technique which creates a well-defined canonical ensemble.

The basic DPD equations are defined in terms of the forces on one particle, which involve two-particle interactions

$$\vec{F}_i^{\text{DPD}} = \sum_{i \neq j} \vec{F}_{ij}^C + \vec{F}_{ij}^D + \vec{F}_{ij}^R \quad (14)$$

with a conservative force \vec{F}_{ij}^C

$$\vec{F}_{ij}^C = -\vec{\nabla}_{ij} U_{ij}(r_{ij}). \quad (15)$$

(where r_{ij} denotes the distance between the centers of particles i and j), a dissipative force \vec{F}_{ij}^D

$$\vec{F}_{ij}^D = -\gamma_{\text{DPD}} \omega_D(r_{ij}) (\hat{r}_{ij} \cdot \vec{v}_{ij}) \hat{r}_{ij} \quad (16)$$

with the friction coefficient γ_{DPD} , and a random force \vec{F}_{ij}^R

$$\vec{F}_{ij}^R = \sqrt{2\gamma_{\text{DPD}} k_B T} \omega_R(r_{ij}) \check{\zeta}_{ij} \hat{r}_{ij}. \quad (17)$$

Here $\check{\zeta}_{ij} = \check{\zeta}_{ji}$ is a symmetric random number with zero mean and unit variance, and the weighting functions of the dissipative and the stochastic force are related by a fluctuation-dissipation theorem,

$$\omega_D(r_{ij}) = [\omega_R(r_{ij})]^2 \equiv \omega_{\text{DPD}}(r_{ij}), \quad (18)$$

which ensures that an equilibrium simulation samples a canonical ensemble^{36,37}. Otherwise, the weight function ω_{DPD} is arbitrary and will be chosen linear here as often in the literature,

$$\omega_{\text{DPD}}(r_{ij}) = \begin{cases} 1 - \frac{r_{ij}}{r_c} & : r_{ij} < r_c \\ 0 & : r_{ij} \geq r_c \end{cases} \quad (19)$$

where r_c denotes the cut-off radius.

B. Tunable slip boundaries

The hydrodynamic boundary condition at the walls is realized with a recently developed method³⁸ that allows to implement arbitrary partial-slip boundary conditions: We introduce an additional coordinate-dependent viscous force that mimicks the wall/fluid friction

$$\mathbf{F}_i^L = \mathbf{F}_i^D + \mathbf{F}_i^R \quad (20)$$

with a dissipative contribution

$$\mathbf{F}_i^D = -\gamma_L \omega_L(z) (\mathbf{v}_i - \mathbf{v}_{\text{wall}}) \quad (21)$$

coupling to the relative velocity ($\mathbf{v}_i - \mathbf{v}_{wall}$) of the particle with respect to the wall, and a stochastic force

$$F_{i,\alpha}^R = \sqrt{2\gamma_L k_B T \omega_L(z)} \chi_{i,\alpha} \quad (22)$$

which satisfies the fluctuation-dissipation relation and thus ensures that the local equilibrium distribution is again a Boltzmann distribution. Here α is $\alpha = x, y, z$ and $\chi_{i,\alpha}$ is a Gaussian distributed random variable with mean zero and variance one: $\langle \chi_{i,\alpha} \rangle = 0$, $\langle \chi_{i,\alpha} \chi_{j,\beta} \rangle = \delta_{ij} \delta_{\alpha\beta}$. The viscous coupling between fluid and wall is achieved by the locally varying viscosity $\gamma_L \omega_L(z)$ with $\omega_L(z) = 1 - z/z_c$ up to a cut-off distance z_c . The prefactor γ_L can be used to tune the strength of the friction force and hence the value of the slip length. Within this approach it is possible to tune the slip length δ_B systematically from full-slip to no-slip, and to derive an analytic expression for the slip length as a function of the model parameters³⁸.

C. Simulation details

We have studied the electrophoresis of charged polymers of length $N = 20$ in electrolyte solutions, confined by a planar slit channel with charged walls. All particles, polymer, solvent and ions, are modeled explicitly. We use a simulation box of size $(12\sigma \times 12\sigma \times 10\sigma)$ which is periodic in x - and y -direction and confined by impermeable walls in the z -direction. The walls repel the particles *via* a soft repulsive WCA potential³⁹ of range σ and amplitude ϵ . (Hence the accessible channel width for the particles is actually $L_z = 8\sigma$). Ions and monomers repel each other with the same WCA potential. In addition, chain monomers are connected by harmonic springs

$$U_{harmonic} = \frac{1}{2} k (r_{ij} - r_0)^2 \quad (23)$$

with the spring constant $k = 25\epsilon/\sigma^2$ and $r_0 = 1.0\sigma$. Neutral solvent particles have no conservative interactions except with the walls.

The wall contains immobilized, negatively charged particles at random positions. Every second monomer on the polyelectrolyte carries a negative charge. The solvent contains the positive counterions for the walls and the polyelectrolyte, and additional (positive and negative) salt ions. All charges are monovalent, and the system as a whole is electroneutral. In addition to their other interactions, charged particles interact *via* a Coulomb potential with the Bjerrum length $\lambda_B = e^2/4\pi\epsilon_r k_B T = 1.0\sigma$, and they are exposed to an external field $E_x = -1.0\epsilon/e\sigma$. Specifically, we have studied systems with a surface charge density of $\sigma_A = -0.208e\sigma^{-2}$. The total counterion density was $\rho = 0.06\sigma^{-3}$ and the salt density varied between $\rho_s = 0.05625, 0.0375, 0.03, 0.025$, and $0.015\sigma^{-3}$.

We use DPD simulations with a friction coefficient $\gamma_{DPD} = 5.0\sigma^{-1}(m\epsilon)^{1/2}$. The density of the solvent particles was $\rho = 3.75\sigma^{-3}$, and the temperature of the system was $T = 1.0\epsilon/k_B$. For these parameters, the shear

Table I: Slip lengths δ_B for different layer friction coefficients γ_L , compared with theoretical value δ_B^T according to Ref. 38.

$\gamma_L[\sigma^{-1}(m\epsilon)^{1/2}]$	$\delta_B[\sigma]$	$\pm\delta_B[\sigma]$	$\delta_B^T[\sigma]$
0.1	14.977	1.879	14.000
0.25	5.664	0.783	5.458
0.5	2.626	0.521	2.613
0.75	1.765	0.409	1.664
1.0	1.292	0.423	1.190
6.1	0.000	0.197	0.000

viscosity of the DPD fluid – as determined by fitting the amplitude of Plane Poiseuille flows³⁸ – is given by $\eta_s = (1.334 \pm 0.003)\sigma^{-2}(m\epsilon)^{1/2}$. The DPD timestep was $\delta t = 0.01\sigma(m/\epsilon)^{1/2}$.

Tunable-slip boundary conditions were used with friction coefficients $\gamma_L = 0.1, 0.25, 0.5, 0.75, 1.0$, and $6.1\sigma^{-1}(m\epsilon)^{1/2}$. The range of the viscous layer was $z_c = 2.0\sigma$. Only the solvent particles interact with the tunable-slip boundaries. By performing Plane Poiseuille and Plane Couette flow simulations with the above given parameters, the slip length δ_B and the hydrodynamic boundary positions z_B can be determined independently³⁸. The hydrodynamic boundary position is found at $|z_B| = (3.866 \pm 0.266)\sigma$ in all simulations. The corresponding slip lengths are presented in Table I together with the theoretical values predicted by the analytic expression in Ref. 38. The comparison shows that the simulated results are in good agreement with the theory.

The electrostatics were calculated by P3M⁴⁰ and the ELC (electrostatic layer correction)-algorithm⁴¹ for $2D + h$ slabwise geometries. All simulations have been carried out with the freely available software package ESPResSo^{42,43}

IV. NUMERICAL RESULTS

Fig. 1 shows the average ionic distributions of anions ρ_a and cations ρ_c for the salt concentration $\rho_s = 0.05625\sigma^{-3}$. Here the 'cations' include the positively charged salt ions and the counterions of the wall and the polyelectrolyte, and the 'anions' only the negatively charged salt ions. Due to the presence of the polyelectrolyte in the middle of the channel, the average cation density there is slightly increased. To determine the inverse effective screening length κ , we have thus fitted the following function

$$\Delta\rho = \Delta\rho_0(e^{-\kappa z} + e^{\kappa z}) + c \quad (24)$$

to the ionic difference $\Delta\rho = \rho_c - \rho_a$. The exponential fit describes the data very well (black solid line in Fig. 1). The fit parameters for κ are listed in Table II, along with

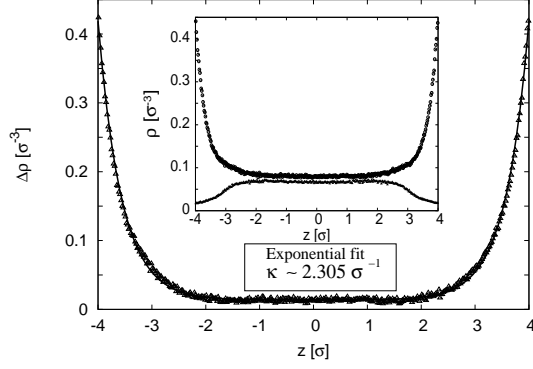


Figure 1: Distribution of the ionic difference $\Delta\rho = \rho_c - \rho_a$ between cations and anions in the solution (not counting the polyelectrolyte) for an exemplary salt concentration of $\rho_s = 0.05625\sigma^{-3}$ and the surface charge density $\sigma_A = -0.208e\sigma^{-2}$. The black line corresponds to an exponential fit (Eq. (24)) with an effective inverse screening length of $\kappa = 2.305 \pm 0.025\sigma^{-1}$. **Inset:** Distribution of cations (circles) and anions (triangles) for the same system.

the values for the Debye-Hückel screening parameter κ_D (Eq. (10)). The decay lengths are overall very different from those predicted by the Debye-Hückel theory. We conclude that the system is outside the validity region of the linearized Poisson-Boltzmann approximation. This is perhaps not surprising, given that the individual ion profiles (inset of Fig. 1) at the walls deviate strongly from their bulk value, *i.e.*, these deviations can hardly be considered as small perturbations. The surface charge is too high. On the other hand, the electrostatic coupling constant $\Xi = 2\pi Z^3 \lambda_B^3 \sigma_A \sim 0.2$ ($Z = 1$ is the valency of the cations) is still much smaller than unity, hence we are still in a ‘weak coupling’ regime. This is also evident from the fact that the effective screening parameter κ differs strongly from the Guy Chapman length, $\mu^{-1} = 2\pi\lambda_B Z \sigma_A = 1.31\sigma$.

The EOF profiles for the same salt concentration ($\rho_s = 0.05625\sigma^{-3}$) are shown in Fig. 2. The different curves correspond to different hydrodynamic boundary conditions (slip lengths). As expected, the flow velocity increases drastically for larger slip lengths. All curves are

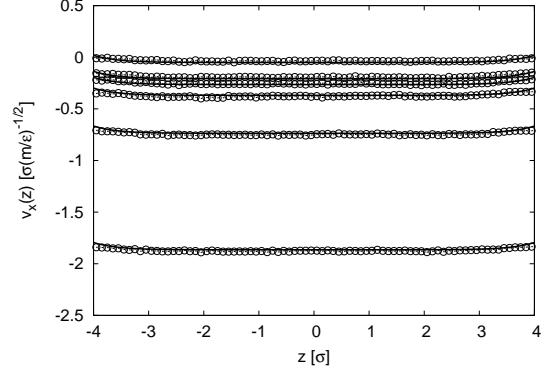


Figure 2: Exemplary flow profiles for a salt concentration $\rho_s = 0.05625\sigma^{-3}$ for varying slip lengths (from bottom to top: $\delta_B = (14.98, 5.66, 2.63, 1.77, 1.29, 0.00)\sigma$.) The black lines are the theoretical predictions obtained by integrating the Stokes equation (Eq. (5)) with a fitted inverse screening length of $\kappa = 2.305\sigma^{-1}$.

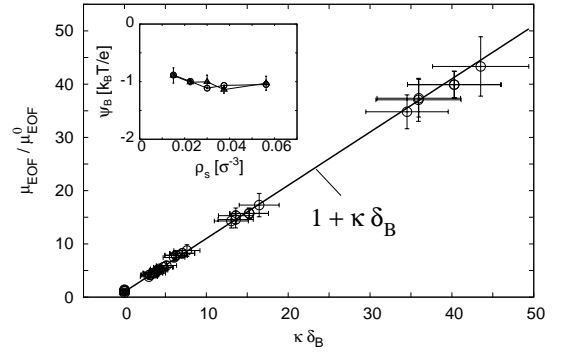


Figure 3: Ratio $\mu_{\text{EOF}}^0/\mu_{\text{EOF}}^0$ plotted against $\delta_B \kappa$ for the different salt concentrations and screening lengths given in Table I and II. The black line is the theoretical prediction of Eq. (7) with slope $1 + \kappa \delta_B$. **Inset:** Surface potential as obtained from μ_{EOF}^0 using Eq. (9) (circles) and independently by a test charge method (triangles) as a function of the salt concentration ρ_s .

Table II: Fitted inverse screening lengths κ and Debye-Hückel screening parameter κ_D for different salt concentrations ρ_s and the fixed counterion density of $\rho = 0.06\sigma^{-3}$.

$\rho_s [\sigma^{-3}]$	$\kappa [\sigma^{-1}]$	$\pm \kappa [\sigma^{-1}]$	$\kappa_D [\sigma^{-1}]$
0.015	1.996	0.041	0.98
0.0225	2.011	0.049	1.02
0.03	1.983	0.041	1.07
0.0375	2.182	0.047	1.11
0.05625	2.305	0.025	1.21

in good agreement with the theoretical predictions, which were obtained by integrating the Stokes equation (24) numerically with the correct partial-slip boundary conditions. In agreement with our earlier studies at zero salt concentration²⁹, we thus find that a description based on the Stokes equation – a continuum equation – remains valid even for very narrow channels.

The flow velocity in the middle of the channel gives the EOF mobility. Fig. 3 compares our numerical results for all salt concentrations and slip lengths with the theoretical prediction of Eq. (7), where μ_{EOF}^0 has been determined by a linear regression for each salt concentration independently. We find good agreement between simulation data and theory. This confirms the validity of our theoretical result, Eq. (7). It also demonstrates that the polyelectrolyte, which was present in all simulations, does not perturb the EOF even in very narrow channels.

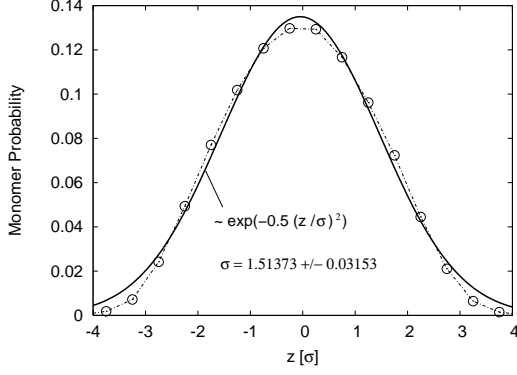


Figure 4: Normalized monomer distribution inside the channel for the salt concentration $\rho_s = 0.05625\sigma^{-3}$.

The values of the EOF mobility for zero slip length, μ_{EOF}^0 , can be used to determine the surface potential ψ_B for the different salt concentrations *via* Eq. (9). As a consistency check, we have also determined ψ_B independently by inserting a test charge into the ion layer at $z = z_B$. The results are shown in the inset of Fig. 3. Both methods give identical results. The surface potential is found to be largely independent of the salt concentration.

After investigating the EOF of the solvent, we discuss the properties of the polyelectrolyte. The probability distribution for finding a monomer at a given position z is shown in Fig. 4 for the salt concentration $\rho_s = 0.05625\sigma^{-3}$. It is approximately Gaussian with a peak in the middle of the channel and a variance $\text{Var} \sim 2.28\sigma$. Thus the polyelectrolyte mainly 'senses' the EOF in the middle of the channel, and the details of the flow profiles close to the channel walls have very little influence on its net mobility: The assumption that the total mobility is governed by a single EOF velocity \mathbf{v}_{EOF} (Eq. (2)) is probably legitimate.

The influence of the ion profiles on the chain structure of the polyelectrolyte can be investigated by considering static properties like the radius of gyration $R_g^2 = (1/2N^2) \sum_{i,j=1}^N \langle (\vec{R}_i - \vec{R}_j)^2 \rangle$ and the end-to-end radius $R_e^2 = \langle (\vec{R}_N - \vec{R}_1)^2 \rangle$ ⁴⁴. The results for these parameters are shown in Table III. Both characteristic

Table III: Radius of gyration R_g and end to end radius R_e for a polyelectrolyte with $N = 20$ monomers for different salt concentrations ρ_s .

$\rho_s[\sigma^{-3}]$	$R_g[\sigma]$	$R_e[\sigma]$
0.015	3.2218 ± 0.047	10.6480 ± 0.0314
0.0225	3.1661 ± 0.0041	10.2736 ± 0.0266
0.03	3.1486 ± 0.0451	10.1777 ± 0.0292
0.0375	3.1279 ± 0.0045	10.0819 ± 0.0287
0.05625	3.0825 ± 0.0045	9.8331 ± 0.0280

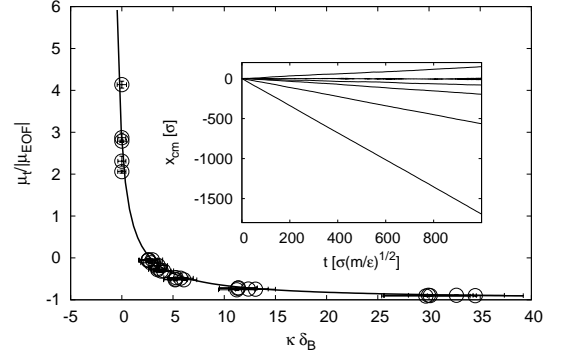


Figure 5: Ratio $\mu_t/|\mu_{\text{EOF}}|$ plotted against $\delta_B \kappa$ for all slip lengths (Table I) and salt concentrations (Table II). The black line is the theoretical prediction of Eqn. (13) with absolute values of $|\mu_{\text{EOF}}|$. In the limit $\delta_B \kappa \rightarrow \infty$, the total mobility of the polyelectrolyte is equal to the electroosmotic mobility μ_{EOF}^0 . The ratio μ_e/μ_{EOF}^0 has been fitted to -3.778 ± 0.128 . Negative values of $\mu_t/|\mu_{\text{EOF}}|$ indicate negative total mobilities of the polyelectrolyte. **Inset:** Total displacement of the polyelectrolytes center of mass for different boundary conditions and a salt concentration of $\rho_s = 0.05625\sigma^{-3}$. The total mobility becomes negative for $|\mu_e| \ll |\mu_{\text{EOF}}|$. The lines correspond from top to bottom to the slip lengths $\delta_B \approx (0.00, 1.292, 1.765, 2.626, 5.664, 14.98)\sigma$. Thus larger slip lengths indirectly enhance the total mobility of the polyelectrolyte.

lengths decrease with increasing salt concentration due to a more effective screening of electrostatic interactions, in accordance with standard theories⁴⁵. The ratio between the end-to-end radii and the gyration radii is unusually large, which is most likely a squeezing effect due to the presence of the channel walls^{46,47}. Specific flow-induced effects such as shear-induced elongation⁴⁸ are probably less important, since the flow profile is basically constant inside the channel. It should be noted that the pure electrophoretic mobility μ_e of the chain is presumably modified by the confinement as an indirect effect of the elongation. This effect has not been investigated in the present study.

The total mobility of the polyelectrolyte for varying boundary conditions and salt concentrations is finally presented in Fig. 5. The theoretical prediction of Eq. (13) agrees well with the numerical results with the single fit parameter $\mu_e/\mu_{\text{EOF}}^0 = -3.778 \pm 0.128$. It is remarkable that this parameter can be set to a constant, *i.e.*, it seems to be largely independent of the salt concentration ρ_s . Since μ_{EOF}^0 does not depend on ρ_s (see Fig. 3, inset), this means that μ_e is also independent of ρ_s for the range of salt concentrations considered here⁴⁹.

For no-slip boundary conditions with $\delta_B \approx 0$, we find ordinary behaviour where the polyelectrolyte follows the applied electric field. In the presence of wall slip, however, the EOF becomes stronger and eventually dominates. Then the total mobility may become negative, *i.e.*, the polyelectrolyte migrates in a direc-

tion which is opposite to the applied force. The inset of Fig. 5 illustrates this by showing the total displacement of the chain's center of mass for the salt concentration $\rho_s = 0.05625\sigma^{-3}$ and various slip lengths. In nearly all cases except $\delta_B \approx 0$, the total mobility of the polyelectrolyte is negative.

To summarize this section, both the assumptions and the predictions of section II are supported by our numerical results. The total mobility of the polyelectrolyte can therefore be adequately described by Eqs. (7) and (13).

V. CONCLUSIONS

We have presented mesoscopic DPD simulations of polyelectrolyte electrophoresis in narrow microchannels, taking full account of hydrodynamic and electrostatic interactions. A particular focus was put on studying the effects of the hydrodynamic boundary conditions at the channel walls on the electroosmotic flow and on the net electrophoretic mobility of the polyelectrolyte. We have shown that they can be incorporated into a single dimensionless parameter $(1 + \kappa \delta_B)$, where δ_B is the slip length and κ the (local) inverse screening length of the charge distribution at the wall. This was derived analytically and supported by our numerical data. It remained valid even for very narrow channels, where the chain conformations were affected by the confinement.

We have shown that wall slip massively enhances the EOF and hence influences the total mobility of the polyelectrolyte. If the EOF mobility μ_{EOF} and the free drain-

ing mobility μ_e oppose each other, *i.e.*, if the effective charges on the polyelectrolyte and the walls have the same sign, the mobility may even become negative. As mentioned in the introduction, this effect has also been observed experimentally⁴. In the other case, where the sign of the charges on the polyelectrolyte and the wall are opposite, the main effect of slip is to enhance the total mobility of the polyelectrolyte.

In summary, the total mobility of polyelectrolytes in microchannels results from an interplay of electroosmotic, electrophoretic, electrostatic and slippage effects. The latter have a particularly strong influence and can be used to design channels with improved properties. For example, the characteristics of the channel walls could be designed to tune effective slip lengths²⁷ and hence flow velocities, which offers the possibility to optimize the time which is needed for polymer migration or separation techniques. This could be an important aspect for future applications in microchannels or micropumps to accelerate measuring times.

Acknowledgments

We thank Christian Holm, Burkhard Dünweg, Ulf D. Schiller, Marcello Sega and Kai Grass for nice and fruitful discussions and the Arminius PC² Cluster at Paderborn University, HLRS Stuttgart and NIC Jülich for computing time. J. S. especially thanks Stefanie Gürtler and Theodor A. Smiatek. Financial funding from the Volkswagen Stiftung is gratefully acknowledged.

* Electronic address: jens.smiatek@uni-muenster.de

† Electronic address: Friederike.Schmid@Uni-Mainz.DE

¹ Viovy, J.-L. *Rev. Mod. Phys.* **2000**, *72*, 813.

² Iki, N.; Kim, Y.; Yeung, E. S. *Anal. Chem.* **1996**, *68*, 4321.

³ Roeraade, M.; Stjernström, M. International Patent WO/1997/26531, **1997**, available at <http://www.wipo.int>.

⁴ Mathe, J.; Di Meglio, J.-M.; Tinland, B. *J. Colloid Interface Sci.* **2007**, *316*, 831.

⁵ Effenhauser, C. S.; Bruin, G. J. M.; Paulus, A. *Electrophoresis* **1997**, *18*, 2203.

⁶ Bader, J. S.; Hammond, R. W.; Henck, S. A.; Deem, M. W.; McDermott, G. A.; Bustillo, J. M.; Simpson, J. W.; Rothberg, J. M. *PNAS* **1999**, *96* 13165.

⁷ Han, J.; Craighead, G. *Science* **2000**, *288*, 1026.

⁸ Han, J.; Turner, S. W.; Craighead, G. *Phys. Rev. Lett.* **2002**, *83*, 1688.

⁹ Huang, L. R.; Tegenfeldt, J. O.; Kraeft, J. J.; Sturm, J. C.; Austin, R. H.; Cox, E. C. *Nature Biotechnology* **2002**, *20*, 1048.

¹⁰ Duong, T. T.; Ros, R.; Streek, M.; Schmid, F.; Brugger, J.; Anselmetti, D.; Ros, A. *Microelectronic Engineering* **2003**, *67-68*, 905.

¹¹ Ros, A.; Hellmich, W.; Duong, T. T.; Anselmetti, D. *J. Biotechnology* **2004**, *112*, 65.

¹² Manning, G. S. *J. Phys. Chem.* **1981**, *85*, 1506.

¹³ Barrat, J.-L.; Joanny, J. F. *J. F. Adv. Chem. Phys.* **1996**, *XCIV*, 1.

¹⁴ Streek, M.; Schmid, F.; Duong, T. T.; Ros, A. *J. Biotechnology* **2004**, *112*, 79.

¹⁵ Streek, M.; Schmid, F.; Duong, T. T.; Ros, A. *Phys. Rev. E* **2005**, *71*, 11905.

¹⁶ Duong-Hong, D.; Han, J.; Wang, J. S.; Hadjiconstantinou, N. G.; Chen, Y. Z.; Liu, G. R. *Electrophoresis* **2008**, *29*, 4880.

¹⁷ Slater, G. W.; Holm, C.; Chubynsky, M. V.; de Haan, H. W.; Dube, A.; Grass, K.; Hickey, O. A.; Kingsburry, C.; Sean, D.; Shendruk, T. N.; Nhan, L. X. *Electrophoresis* **2009**, *30*, 792.

¹⁸ Long, D.; Viovy, J.-L.; Ajdari, A. *Phys. Rev. Lett.* **1996**, *76*, 3858.

¹⁹ Grass, K.; Böhme, U.; Scheler, U.; Cottet, H.; Holm, C. *Phys. Rev. Lett.* **2008**, *100*, 096104.

²⁰ Frank, S.; Winkler, R. G. *Europhys. Lett.* **2008**, *83*, 38004.

²¹ Cummings, E. B.; Griffiths, S. K.; Nilson, R. H.; Paul, P. H. *Anal. Chem.* **2000**, *72*, 2526.

²² We note that it is always possible to separate a steady velocity field $\mathbf{v}(\mathbf{r})$ into an EOF component $\mathbf{v}_{\text{EOF}}(\mathbf{r})$ which satisfies the EOF boundary conditions, and a residual (e.g., Poiseuille flow) component with no-slip boundary conditions at the wall and arbitrary boundary conditions at the

- inlet and outlet of the channel.
- ²³ Hunter, R. J., *Foundations of Colloid Science*; Clarendon Press: Oxford, 1991.
 - ²⁴ Pit, R.; Hervet, H.; Leger, L. *Phys. Rev. Lett.* **2000**, *85*, 980.
 - ²⁵ Tretheway, D.; Meinhart, C. *Physics of Fluids* **2002**, *14*, 9.
 - ²⁶ Neto, C.; Evans, D. R.; Bonaccorso, E.; Butt, H.-J.; Craig, V. S. J. *Rep. Prog. Phys.* **2005**, *68*, 2859.
 - ²⁷ Barrat, J.-L.; Boquet, L. *Soft Matter* **2007**, *3*, 685.
 - ²⁸ Joly, L.; Ybert, C.; Trizac, E.; Bocquet, L. *Phys. Rev. Lett.* **2004**, *93*, 257805.
 - ²⁹ Smiatek, J.; Sega, M.; Schiller, U. D.; Holm, C.; Schmid, F. *J. Chem. Phys.* **2009**, *130*, 244702.
 - ³⁰ Lu, P.-C. *Introduction to the mechanics of viscous fluids*; Holt, Rinehart and Winston Inc.: New York, 1973.
 - ³¹ Israelachvili, J. *Intermolecular and Surface Forces*; Academic Press: London, 1991.
 - ³² Mitchell, D. J.; Ninham, B. W. *Chem. Phys. Lett.* **1978**, *53*, 397.
 - ³³ Kjellander, R.; Mitchell, D. J. *J. Chem. Phys.* **1994**, *101*, 603.
 - ³⁴ McBride, A.; Kohonen, M.; Attard, P. *J. Chem. Phys.* **1998**, *109*, 2423.
 - ³⁵ Moreira, A. G.; Netz, R. R. *Europhys. Lett.* **2002**, *52*, 705.
 - ³⁶ Español, P.; Warren, P. B. *Europhys. Lett.* **1995**, *30*, 191.
 - ³⁷ Groot, R. D.; Warren, P. B. *J. Chem. Phys.* **1997**, *107*, 4423.
 - ³⁸ Smiatek, J.; Allen, M. P.; Schmid, F. *Eur. Phys. J. E* **2008**, *26*, 115.
 - ³⁹ Weeks, J. D.; Chandler, D.; Andersen, H. C. *J. Chem. Phys.* **1971**, *54*, 5237.
 - ⁴⁰ Hockney, R. W.; Eastwood, J. W. *Computer simulation using particles*; McGraw-Hill: New York, 1981.
 - ⁴¹ Arnold, A.; de Joannis, J.; Holm, C. *J. Chem. Phys.* **2002**, *117*, 2496.
 - ⁴² ESPResSo-Homepage, <http://www.espresso.mpg.de> (2002-2010).
 - ⁴³ Arnold, A.; Mann, B. A.; Limbach, H.-J.; Holm, C. *Comp. Phys. Comm.* **1005**, *174*, 704.
 - ⁴⁴ Doi, M.; Edwards, S. F. *The Theory of Polymer Dynamics*; Oxford Science Publications: Oxford, 1986.
 - ⁴⁵ Dobrynin, A. V.; Rubinstein, M. *Prog. Polym. Sci.* **2005**, *30*, 1049.
 - ⁴⁶ de Gennes, P.-G. *Scaling concepts in polymer physics*; Cornell press: Ithaca, 1979.
 - ⁴⁷ Cannavacciuolo, L.; Winkler, R. G.; Gompfer, G. *Europhys. Lett.* **2008**, *83*, 34007.
 - ⁴⁸ Boroudjerdi, H.; Kim, Y.-W.; Naji, A.; Netz, R. R.; Schlagberger, X.; Serr, A. *Phys. Rep.* **2005**, *416*, 129.
 - ⁴⁹ Muthukumar, M. *J. Chem. Phys.* **1997**, *107*, 2619.